Journal of Organometallic Chemistry 886 (2019) 48–56

Contents lists available at ScienceDirect

Journal of Organometallic Chemistry

journal homepage: www.elsevier.com/locate/jorganchem

Palladium(II) and ruthenium(II) complexes of benzotriazole functionalized *N*-heterocyclic carbenes: Cytotoxicity, antimicrobial, and DNA interaction studies

Gülnihan Onar [a], Canbolat Gürses [b], Mert Olgun Karataş [a, *], Sevgi Balcıoğlu [a], Nuriye Akbay [c], Namık Özdemir [d], Burhan Ateş [a], Bülent Alıcı [a]

[a] İnönü University, Faculty of Arts and Science, Department of Chemistry, Malatya, Turkey
[b] İnönü University, Faculty of Arts and Science, Department of Molecular Biology and Genetics, Malatya, Turkey
[c] İstanbul Medeniyet University, Faculty of Engineering and Natural Sciences, Department of Chemistry, Istanbul, Turkey
[d] Ondokuz Mayıs University, Faculty of Education, Department of Mathematics and Science Education, Samsun, Turkey

ARTICLE INFO

Article history:
Received 24 January 2019
Received in revised form
7 February 2019
Accepted 13 February 2019
Available online 16 February 2019

Keywords:
Benzotriazole
Palladium(II)
Ruthenium(II)
N-heterocyclic carbene
Anticancer
Antimicrobial

ABSTRACT

In the present study, four palladium and four ruthenium complexes were synthesized with benzotriazole substituted *N*-heterocyclic carbene ligands. The structures of complexes were established by appropriate spectroscopic methods and elemental analyses. In addition, the crystal structure of a Pd–NHC complex (**1c**) was reported. Anticancer, antimicrobial and DNA interaction properties of the complexes were examined. Antimicrobial effects of the complexes were tested against two bacteria strains and one fungi strain. Cytotoxic effects of the complexes were tested against human breast (MCF-7) and colorectal (Caco-2) cancer cell lines and non-cancer mouse fibroblast (L-929) cell lines. Ruthenium complexes were found as more cytotoxic than palladium complexes against cancer cell lines. Especially, benzyl containing, benzimidazole-based ruthenium complexes (**3c** and **3d)** were found as non-cytotoxic against non-cancer L-929 cell lines while performing comparable cytotoxicity against Caco-2 cancer cell lines with cisplatin. In addition, DNA interaction studies were performed with pBR322 plasmid DNA and *ct*DNA and results showed that both palladium and ruthenium complexes have weaker ability to interact with DNA than cisplatin. The results from this study showed that although the cytotoxic properties of the complexes are not stronger than cisplatin, selectivity of benzyl containing benzimidazole-based ruthenium-NHC complexes against Caco-2 cell lines provides them an advantage, and they deserve further research in the treatment of human colorectal cancer.

1. Introduction

The success achieved by the application of cisplatin in cancer treatment led to the research of metal-organic and organometallic complexes, and inorganic compounds in modern medicine as drug candidates [1]. Investigation of these compounds mainly focused on the treatment of cancer and bacterial infections. For this purpose, many transition metal complexes with various types of ligands have been prepared for the last four decades [2]. Coordination numbers of transition metals ranging from two to ten allow structural diversity for drug design. Additionally, in organometallic complexes, strong metal-carbon bond increases the stability which is highly important for the biological activities of the complexes [3]. Although most investigated organometallic complexes are metallocenes, metal-arene and metal-carbonyl complexes, *N*-heterocyclic carbene (NHC) complexes are the new and promising member of organometallic complexes for drug design [4].

The first metal-NHC complexes were synthesized by Wanzlick and Schönherr [5], and Öfele [6] in 1968, however, research into NHC chemistry rapidly increased after the isolation of the first stable free NHC by Arduengo et al., in 1991 [7]. In the first years, chemists mainly focused on the synthesis and catalytic properties of NHC complexes [8]. According to the literature, the first study about the biological activities of NHC complexes was reported by Çetinkaya and co-workers. They reported the antibacterial properties of ruthenium and rhodium NHC complexes [9]. In 2004,

* Corresponding author.
E-mail addresses: mert.karatas@inonu.edu.tr, mertolgunkaratas@gmail.com (M.O. Karataş).

https://doi.org/10.1016/j.jorganchem.2019.02.013
0022-328X/

silver-NHC complexes were reported as new antibacterial agents by Youngs et al. [10] and anti-tumour activities of cationic gold(I)–NHCs were displayed by Barnard et al. [11]. These pioneering studies launched the investigation of metal-NHC complexes as anticancer and antibacterial agents by many research groups [4].

In recent years, one of the new ideas is the biological evaluation of metal complexes with functionalized NHC ligands. The main goal of this idea is increasing the effectiveness and bio-conjugation of complexes by introducing biologically relevant substituents to NHC scaffold. A number of research groups including our group synthesized the functionalized NHC complexes and investigated their biological properties for this purpose [12]. Benzotriazole is a biologically active heterocycle [13] and triazole core is one of the moieties used for the functionalization of NHCs [14]. Our group recently reported the synthesis and biological evaluation of benzotriazole functionalized silver-NHC complexes and stronger cytotoxicities were observed against human breast and colorectal cancer cell lines in compare with cisplatin [15]. After the promising results achieved with silver-NHCs and reported significant biological activities of palladium and ruthenium complexes, we decided to synthesize benzotriazole functionalized ruthenium and palladium NHC complexes and evaluate their biological activities.

Although platinum, gold, and silver NHC complexes are most investigated, it is known that some ruthenium [16] and palladium [17] NHC complexes also perform significant anticancer effects. On the other hand, ruthenium and palladium NHC complexes perform lower antibacterial effects in comparison with their rhodium [9], silver and gold derivatives [17], respectively. Some ruthenium-based arene and *N*-coordinated complexes are capable of overcoming the resistance induced by platinum drugs in cancer cells [4]. However, the mechanisms of action of ruthenium NHCs as well as other ruthenium anticancer complexes remains unclear. Results indicate that ruthenium complexes may inhibit enzymes or induces the dysfunction of mitochondria [18]. Additionally, some studies demonstrated that ruthenium complexes have more favourable toxicological profile than corresponding gold and platinum complexes [4,19]. On the other hand, palladium is another important metal in medicinal research due to significant similarities of the coordination chemistry with platinum. Some studies showed that the main target of palladium NHCs in cancer cells is DNA similar to cisplatin [17,20]. However detailed investigation is necessary in order to understand the mechanisms of action of palladium-based complexes.

In the present study, based on the above information, we aimed the synthesis of benzotriazole functionalized NHCs complexes of ruthenium and palladium in order to investigate their biological properties. For this purpose, novel four ruthenium and four palladium complexes were synthesized and characterized. Anticancer properties of the complexes were tested against human breast (MCF-7) and colorectal (Caco-2) cancer and mouse fibroblast (L-929) cell lines. Antimicrobial activities of complexes were tested against *Escherichia coli, Bacillus subtilis* bacterial strains and *Candida albicans* fungi. DNA interaction properties of the ruthenium and palladium NHC complexes were examined by using pBR322 plasmid DNA in agarose gel electrophoresis method and following the effect of complexes on UV–visible absorption spectra and fluorescence emission of ethidium bromide-*ct*DNA system.

2. Experimental

2.1. General considerations

Imidazolium and benzimidazolium salts [21], and silver-NHC complexes [15] were available from our previous studies. Synthesis of Pd(II)–NHC complexes were carried out under open air conditions. Synthesis of Ru(II)–NHC complexes were carried out under dry argon atmosphere with rigorous exclusion of air using Schlenk tube techniques. $PdCl_2$ and $[Ru(p\text{-cymene})Cl_2]_2$ were purchased from Aldrich Chem. Co (Istanbul, Turkey). All solvents were provided as commercially, and dichloromethane (DCM) and *n*-hexane were distilled over P_2O_5 before use. Melting points were determined in open capillary tubes by Electrothermal-9200 melting point apparatus. The C, H and N elemental analyses were determined by LECO CHNS-932 elemental analyser. IR spectra were obtained in ATR Sampling Accessory with Perkin Elmer Spectrum 100 Spectrophotometer (400-4000 cm^{-1}). The ^1H and ^{13}C NMR spectra were recorded using Bruker UltraShield 300 operating at 300 MHz (^1H) and 75 MHz (^{13}C), and Bruker Ascend™ 400 Avance III HD operating at 400 MHz (^1H) and 100 MHz (^{13}C). Chemical Shifts (expressed in part per million (ppm)) are referenced to Tetramethylsilane (TMS). Coupling constants, *J*, are given in Hz. NMR multiplicities are abbreviated as follows: s = singlet, d = doublet, t = triplet, q = quartet, quin = quintet, sex = sextet, sep = septet, m = multiplet. Spectral assignments for NHC complexes were achieved by the combination of $^1H–^1H$ COSY and $^1H–^{13}C$ HSQC and $^1H–^{13}C$ HMBC experiments.

2.2. Synthesis and characterization data

Synthesis of Pd(II)–NHC complexes, 1a-d. A solution of corresponding carbene precursor (0.45 mmol), $PdCl_2$ (0.45 mmol) and K_2CO_3 (2.5 mmol) in pyridine (5 mL) was stirred at 80 °C for 3 h. After this period of time, unreacted pyridine was removed under vacuum. 5 mL of DCM was added to mixture and the mixture was passed through silica gel and Celite® column. The final DCM solution of target complex was concentrated to ca. 5 mL and 5 mL of *n*-hexane was added to the mixture. Obtained crystals were collected by filtration, washed with *n*-hexane (3 × 5 mL) and dried under vacuum.

[1-Methyl-3-((1*H*-benzo[*d*]1,2,3-triazole-1-yl)methyl)imidazol-2-ylidene](pyridine) palladium(II) dichloride, 1a. Yellow solid, yield: 75 mg (36%), mp: 240–244 °C. Anal. Calcd. for $C_{16}H_{16}Cl_2N_6Pd$: C, 40.9; H, 3.4; N, 17.9. Found: C, 41.1; H, 3.6; N, 18.0. IR (cm^{-1}): 3166, 3127, 3007, 1709, 1604, 1575, 1472, 1446. ^1H NMR (300 MHz, DMSO-d_6, 298 K): 8.83 (d, 2H, *J* = 5.0 Hz, Py**H**-*o*), 8.38 (d, 1H, *J* = 8.4 Hz, Ar**H**), 8.17 (d, 1H, *J* = 8.3 Hz, Ar**H**), 8.07 (m, 1H, Py**H**-*p*), 7.84 (d, 1H, *J* = 1.8 Hz, $\mathbf{H}_{imidazole}$), 7.65 (m, 2H, Py**H**-*m*), 7.60 (t, 1H, *J* = 7.5 Hz, Ar**H**), 7.53 (d, 1H, *J* = 1.8 Hz, $\mathbf{H}_{imidazole}$), 7.49 (t, 1H, *J* = 7.6 Hz, Ar**H**), 7.40 (s, 2H, NC$\mathbf{H}_2$N), 4.05 (s, 3H, NC$\mathbf{H}_3$). ^{13}C NMR (75 MHz, DMSO-d_6, 298 K): 151.7 (Pd-$\mathbf{C}_{carbene}$), 151.4, 145.9, 139.4, 132.9, 128.3, 125.4, 124.9, 124.8, 123.5, 119.9, 111.7, 60.2 (N$\mathbf{C}H_2$N), 38.2 (N$\mathbf{C}H_3$).

[1-Butyl-3-((1*H*-benzo[*d*]1,2,3-triazole-1-yl)methyl)imidazol-2-ylidene](pyridine) palladium(II) dichloride, 1b. Yellow solid, yield: 110 mg (48%), mp: 173–175 °C (Decomposition). Anal. Calcd. for $C_{19}H_{22}Cl_2N_6Pd$: C, 44.6; H, 4.3; N, 16.4. Found: C, 44.8; H, 4.5; N, 16.5. IR (cm^{-1}): 3108, 2962, 2874, 1602, 1471, 1448. ^1H NMR (300 MHz, $CDCl_3$, 298 K): 9.05 (d, 2H, *J* = 5.1 Hz, Py**H**-*o*), 8.44 (d, 1H, *J* = 8.3 Hz, Ar**H**), 8.09 (d, 1H, *J* = 8.3 Hz, Ar**H**), 7.84 (m, 1H, Py**H**-*p*), 7.55 (t, 1H, *J* = 7.7 Hz, Ar**H**), 7.48–7.38 (m, 5H, NC$\mathbf{H}_2$N (2H), Py**H**-*m* (2H), Ar**H** (1H)), 6.99 (d, 1H, *J* = 1.9 Hz, $\mathbf{H}_{imidazole}$), 6.93 (d, 1H, *J* = 1.9 Hz, $\mathbf{H}_{imidazole}$), 4.59 (t, 2H, *J* = 7.5 Hz, NC$\mathbf{H}_2CH_2$), 2.08 (quin, 2H, *J* = 7.5 Hz, $NCH_2\mathbf{C}H_2$), 1.50 (sex, 2H, *J* = 7.5 Hz, $C\mathbf{H}_2CH_3$), 1.04 (t, 3H, *J* = 7.3 Hz, $CH_2C\mathbf{H}_3$). ^{13}C NMR (75 MHz, $CDCl_3$, 298 K): 151.3, 150.9 (Pd-$\mathbf{C}_{carbene}$), 146.4, 138.4, 133.5, 128.7, 124.9, 124.7, 123.1, 120.5, 120.0, 111.1, 60.8 (N$\mathbf{C}H_2$N), 51.3 (N$\mathbf{C}H_2CH_3$), 32.6 ($NCH_2\mathbf{C}H_2$), 19.9 ($\mathbf{C}H_2CH_3$), 13.8 ($CH_2\mathbf{C}H_3$).

[1-Butyl-3-((1*H*-benzo[*d*]1,2,3-triazole-1-yl)methyl)benzimidazol-2-ylidene](pyridine) palladium(II) dichloride, 1c. Yellow solid, yield: 140 mg (55%), mp: 241–243 °C. Anal. Calcd. for

$C_{23}H_{24}Cl_2N_6Pd$: C, 49.2; H, 4.3; N, 15.0. Found: C, 49.4; H, 4.4; N, 15.1. IR (cm^{-1}): 3110, 2953, 1606, 1481, 1449. ^1H NMR (300 MHz, $CDCl_3$, 298 K): 9.08 (m, 2H, Py**H**-*o*), 8.71 (d, 1H, $J = 8.3$ Hz, Ar**H**), 8.06 (d, 1H, $J = 8.3$ Hz, Ar**H**), 7.86 (m, 1H, Py**H**-*p*), 7.78 (s, 2H, NC**H**$_2$N), 7.74–7.71 (m, 1H, Ar**H**), 7.54–7.22 (m, 7H, Py**H**-*m* (2H), Ar**H** (5H)), 4.93 (t, 2H, $J = 7.7$ Hz, NC**H**$_2$CH$_2$), 2.24 (quin, 2H, $J = 7.6$ Hz, NCH$_2$C**H**$_2$), 1.63 (m, 2H, C**H**$_2$CH$_3$), 1.10 (t, 3H, $J = 7.3$ Hz, CH$_2$C**H**$_3$). ^{13}C NMR (75 MHz, $CDCl_3$, 298 K): 164.8 (Pd-**C**$_{carbene}$), 151.3, 146.4, 138.5, 134.6, 133.8, 132.6, 128.5, 124.8, 124.7, 124.3, 124.2, 119.9, 111.9, 111.6, 110.7, 60.5 (N**C**H$_2$N), 48.7 (N**C**H$_2$CH$_2$), 31.6 (NCH$_2$**C**H$_2$), 20.3 (**C**H$_2$CH$_3$), 13.9 (CH$_2$**C**H$_3$).

[1-Benzyl-3-((1*H*-benzo[*d*]1,2,3-triazole-1-yl)methyl)benzimidazol-2-ylidene](pyridine) palladium(II) dichloride, 1d. Yellow solid, yield: 140 mg (52%), mp: 212–215 °C. Anal. Calcd. for $C_{26}H_{22}Cl_2N_6Pd$: C, 52.4; H, 3.7; N, 14.1. Found: C, 52.6; H, 3.9; N, 14.3. IR (cm^{-1}): 3041, 1606, 1479, 1448. ^1H NMR (400 MHz, $CDCl_3$, 298 K): 9.04 (m, 2H, Py**H**-*o*), 8.78 (d, 1H, $J = 8.3$ Hz, Ar**H**), 8.08 (d, 1H, $J = 8.3$ Hz, Ar**H**), 7.83 (m, 3H, NC**H**$_2$N (2H) and Py**H**-*p* (1H)), 7.75 (d, 1H, $J = 8.0$ Hz, Ar**H**), 7.60–7.11 (m, 12H, Ar**H**), 6.24 (s, 2H, NC**H**$_2$Ph). ^{13}C NMR (100 MHz, $CDCl_3$, 298 K): 166.1 (Pd-**C**$_{carbene}$), 151.3, 146.4, 138.5, 134.7, 134.4, 134.0, 132.6, 129.0, 128.6, 128.4, 127.9, 124.8, 124.5, 124.3, 120.0, 111.9, 111.7, 111.6, 60.5 (N**C**H$_2$N), 53.4 (N**C**H$_2$Ph).

Synthesis of Ru(II)–NHC complexes (3a-d). A solution (20 mL) of corresponding Ag(I)–NHC (0.13 mmol) and [RuCl$_2$(p-cymene)]$_2$ (0.13 mmol) in DCM (20 mL) was stirred at 40 °C for 24 h. After this period, the mixture was filtered through Celite®, solvent and volatile components were removed under reduced pressure. The crude product was washed with *n*-hexane (2 × 10 mL) and dried under vacuum.

Dichloro[1-butyl-3-((1*H*-benzo[*d*]1,2,3-triazole-1-yl)methyl) imidazol-2-ylidene](*p*-cymene) ruthenium(II), 3a. Orange solid, yield: 70 mg (48%), mp: 158–160 °C (Decomposition). Anal. Calcd. for $C_{24}H_{31}Cl_2N_5Ru$: C, 51.3; H, 5.6; N, 12.5. Found: C, 51.6; H, 5.6; N, 12.2. IR (cm^{-1}): 2959, 1615, 1496, 1451, 1424. ^1H NMR (300 MHz, DMSO-d_6, 298 K): 8.26 (d, 1H, $J = 8.5$ Hz, Ar**H**), 8.17 (d, 1H, $J = 8.5$ Hz, Ar**H**), 8.02 (d, 1H, $J = 1.8$ Hz, **H**$_{imidazole}$), 7.79 (d, 1H, $J = 14.1$ Hz, NC**H**$_2$N), 7.75 (d, 1H, $J = 1.8$ Hz, **H**$_{imidazole}$), 7.72 (m, 1H, Ar**H**), 7.55 (m, 1H, Ar**H**), 6.17 (d, 1H, $J = 14.1$ Hz, NC**H**$_2$N), 6.06 (d, 1H, $J = 6.0$ Hz, Ar**H**-*p*-cymene), 5.93 (m, 2H, Ar**H** (*p*-cymene)), 5.72 (d, 1H, $J = 6.0$ Hz, Ar**H** (*p*-cymene)), 4.18 (t, 2H, $J = 8.0$ Hz, NC**H**$_2$CH$_2$), 2.88 (sep, 1H, $J = 6.8$ Hz, C**H**(CH$_3$)$_2$), 2.13 (s, 3H, ArC**H**$_3$), 1.91–1.67 (m, 2H, NCH$_2$C**H**$_2$), 1.38 (m, 2H, C**H**$_2$CH$_3$), 1.24 (m, 6H, CH(C**H**$_3$)$_2$), 0.94 (t, 3H, $J = 7.3$ Hz, CH$_2$C**H**$_3$). ^{13}C NMR (75 MHz, DMSO-d_6, 298 K): 173.3 (Ru-**C**$_{carbene}$), 145.1, 134.0, 129.6, 125.9, 122.8, 122.0, 118.6, 112.4, 110.5, 102.5, 87.9, 87.5, 87.3, 83.4, 58.9 (N**C**H$_2$N), 50.0 (N**C**H$_2$CH$_2$), 32.1 (NCH$_2$**C**H$_2$), 30.7 (**C**H(CH$_3$)$_2$), 23.3 and 20.6 (CH(**C**H$_3$)$_2$), 19.5 (**C**H$_2$CH$_3$), 18.4 (Ar**C**H$_3$), 13.7 (CH$_2$**C**H$_3$).

Dichloro[1-butyl-3-((1*H*-benzo[*d*]1,2,3-triazole-1-yl)methyl) benzimidazol-2-ylidene](*p*-cymene) ruthenium(II), 3b. Orange solid, yield: 90 mg (57%), mp: 154–156 °C (Decomposition). Anal. Calcd. for $C_{28}H_{33}Cl_2N_5Ru$: C, 55.0; H, 5.4; N, 11.5. Found: C, 55.2; H, 5.6; N, 11.1. IR (cm^{-1}): 2960, 1612, 1488, 1412. ^1H NMR (300 MHz, DMSO-d_6, 298 K): 8.64 (d, 1H, $J = 8.5$ Hz, Ar**H**), 8.53 (d, 1H, $J = 7.9$ Hz, Ar**H**), 8.20 (d, 1H, $J = 8.5$ Hz, Ar**H**), 7.95 (d, 1H, $J = 14.6$ Hz, NC**H**$_2$N), 7.85 (d, 1H, $J = 7.9$ Hz, Ar**H**), 7.78 (m, 1H, Ar**H**), 7.60–7.43 (m, 3H, Ar**H**), 6.38 (d, 1H, $J = 14.6$ Hz, NC**H**$_2$N), 6.19 (d, 1H, $J = 6.0$ Hz, Ar**H** (*p*-cymene)), 6.11–6.02 (m, 2H, Ar**H** (*p*-cymene)), 5.89 (d, 1H, $J = 6.0$ Hz, Ar**H** (*p*-cymene)), 4.52 (m, 2H, NC**H**$_2$CH$_2$), 2.96 (sep, 1H, $J = 6.9$ Hz, C**H**(CH$_3$)$_2$), 2.16 (s, 3H, ArC**H**$_3$), 1.91 (m, 2H, NCH$_2$C**H**$_2$), 1.53 (m, 2H, C**H**$_2$CH$_3$), 1.29 (m, 6H, CH(C**H**$_3$)$_2$), 1.00 (t, 3H, $J = 7.3$ Hz, CH$_2$C**H**$_3$). ^{13}C NMR (75 MHz, DMSO-d_6, 298 K): 188.3 (Ru-**C**$_{carbene}$), 145.2, 134.3, 133.6, 133.5, 129.7, 126.0, 123.9, 118.6, 114.3, 111.9, 111.3, 110.9, 102.8, 89.2, 89.1, 87.3, 84.0, 56.9 (N**C**H$_2$N), 48.9 (N**C**H$_2$CH$_2$), 31.3 (NCH$_2$**C**H$_2$), 30.7 (**C**H(CH$_3$)$_2$), 22.9 and 20.9 (CH(**C**H$_3$)$_2$), 19.7 (**C**H$_2$CH$_3$), 18.4 (Ar**C**H$_3$), 13.7 (CH$_2$**C**H$_3$).

Dichloro[1-benzyl-3-((1*H*-benzo[*d*]1,2,3-triazole-1-yl) methyl)benzimidazol-2-ylidene](*p*-cymene) ruthenium(II), 3c. Orange solid, yield: 70 mg (42%), mp: 163–165 °C (Decomposition). Anal. Calcd. for $C_{31}H_{31}Cl_2N_5Ru$: C, 57.7; H, 4.8; N, 10.9. Found: C, 57.8; H, 5.0; N, 10.5. IR (cm^{-1}): 2962, 1611, 1497, 1450, 1416. ^1H NMR (400 MHz, DMSO-d_6, 298 K): 8.71 (d, 1H, $J = 8.4$ Hz, Ar**H**), 8.60 (d, 1H, $J = 8.2$ Hz, Ar**H**), 8.23 (d,1H, $J = 8.5$ Hz, Ar**H**), 8.07 (d, 1H, $J = 14.6$ Hz, NC**H**$_2$N), 7.81 (m, 1H, Ar**H**), 7.61 (m, 1H, Ar**H**), 7.49 (m, 1H, Ar**H**), 7.39–7.21 (m, 7H, Ar**H**), 6.46 (d, 1H, $J = 14.6$ Hz, NC**H**$_2$N), 6.14–5.70 (m, 6H, NC**H**$_2$Ph (2H) and Ar**H** (*p*-cymene, 4H)), 2.96 (sep, 1H, $J = 6.7$ Hz, C**H**(CH$_3$)$_2$), 2.14 (s, 3H, ArC**H**$_3$), 1.33–1.20 (m, 6H, CH(C**H**$_3$)$_2$). ^{13}C NMR (100 MHz, DMSO-d_6, 298 K): 189.8 (Ru-**C**$_{carbene}$), 145.2, 136.3, 134.3, 134.0, 133.7, 129.7, 128.7, 127.8, 126.7, 126.0, 123.9, 118.6, 114.9, 112.0, 111.5, 111.0, 101.9, 89.6, 88.2, 87.4, 84.2, 57.1 (N**C**H$_2$N), 52.0 (N**C**H$_2$Ph), 30.6 (**C**H(CH$_3$)$_2$), 22.9 and 20.6 (CH(**C**H$_3$)$_2$), 18.5 (Ar**C**H$_3$).

Dichloro[1-(3,4,5-trimethoxybenzyl)-3-((1*H*-benzo[*d*]1,2,3-triazole-1-yl)methyl)benzimidazol-2-ylidene](*p*-cymene) ruthenium(II), 3d. Orange solid, yield: 75 mg (39%), mp: 142–144 °C (Decomposition). Anal. Calcd. for $C_{34}H_{37}Cl_2N_5O_3Ru$: C, 55.5; H, 5.1; N, 9.5. Found: C, 55.8; H, 5.2; N, 9.2. IR (cm^{-1}): 2961, 1614, 1441, 1418. ^1H NMR (300 MHz, DMSO-d_6, 298 K): 8.68 (m, 1H, Ar**H**), 8.56 (m, 1H, Ar**H**), 8.23 (d, 1H, $J = 8.4$ Hz, Ar**H**), 8.01 (d, 1H, $J = 14.5$ Hz, NC**H**$_2$N), 7.95 (s, 1H, Ar**H**), 7.80 (m, 1H, Ar**H**), 7.59 (m, 1H, Ar**H**), 7.50 (m, 1H, Ar**H**), 7.35 (m, 2H, Ar**H**), 6.71 (s, 2H, Ar**H**), 6.43 (d, 1H, $J = 14.5$ Hz, NC**H**$_2$N), 6.13–5.79 (m, 6H, NC**H**$_2$N (2H) and Ar**H** (*p*-cymene, 4H)), 3.67 (s, 9H, ArOC**H**$_3$), 2.97 (sep, 1H, $J = 6.7$ Hz, C**H**(CH$_3$)$_2$)), 2.18 (s, 3H, ArC**H**$_3$), 1.31 and 1.23 (both d, 6H, $J = 6.7$ Hz, CH(C**H**$_3$)$_2$). ^{13}C NMR (100 MHz, DMSO-d_6, 298 K): 189.9 (Ru-**C**$_{carbene}$), 153.1, 145.2, 137.0, 134.3, 134.1, 133.7, 131.6, 129.7, 126.0, 124.01, 123.98, 118.6, 114.8, 112.1, 111.5, 111.0, 104.7, 102.2, 89.5, 88.0, 87.9, 84.2, 60.1 (ArO**C**H$_3$), 57.0 (N**C**H$_2$N), 56.0 (ArO**C**H$_3$), 52.4 (N**C**H$_2$Ph), 30.6 (**C**H(CH$_3$)$_2$), 23.1 and 20.5 (CH(**C**H$_3$)$_2$), 18.6 (Ar**C**H$_3$).

2.3. X-ray analysis

Intensity data of **1c** were collected on a STOE IPDS II diffractometer at room temperature using graphite-monochromated Mo Kα radiation by applying the ω-scan method. Data collection and cell refinement were carried out using X-AREA [22] while data reduction was applied using X-RED32 [22]. The structure was solved by a dual-space algorithm using SHELXT-2014 [23] and refined with full-matrix least-squares calculations on F^2 using SHELXL-2017 [24] implemented in WinGX [25] program suit. All H atoms were placed in geometrically idealized positions and constrained to ride on their parent atoms with C–H distances at 0.93, 0.97 and 0.96 Å for CH, CH$_2$ and CH$_3$ atoms, respectively. The butyl moiety is disordered over two positions with a site-occupancy ratio of 0.706(6):0.294(6)%. Crystal data, data collection and structure refinement details are summarized in Table S1. The molecular graphic was drawn by using ORTEP-3 [25].

2.4. Cytotoxicity studies

MCF-7 and Caco-2 cell lines were supplied from Bilkent University Institute of Materials Science and Nanotechnology UNAM | National Nanotechnology Research Centre and sub-cultured in İnönü University, Cell Culture Lab of Chemistry Department. L-929 cell line was supplied from Hacettepe University, Cell Culture Lab of Chemistry Department and sub-cultured in İnönü University, Cell Culture Lab of Chemistry Department. The MCF-7, Caco-2 and L-929 cell lines used for the assay were incubated in DMEM medium at 37 °C in a 5% CO_2 atmosphere until the cells were 80% confluent. Cells were then removed by trypsin and counted with the Thoma slide. Then, the cells were seeded to 96-well plates

($7*10^3$ cells/well for MCF-7, $8*10^3$ cells/well for Caco-2, and $7*10^3$ cells/well for L-929) and incubated at the same conditions for 24 h. Samples were prepared at different concentrations with DMEM (contains less than 1% dimethyl sulfoxide (DMSO)) and added to the wells after removing the media and incubated 24 h under the same conditions. Compound solutions were removed from the cells and replaced with media/MTT (5 mg/ml in PBS) (9:1). After incubation for 4 h in the dark under the same conditions, the mixture was removed from the cells and 100 μl DMSO was added. Then, the absorbance was measured at 550 nm by EON C microplate reader and % viability and IC_{50} values were calculated. Control wells were accepted as 100% live.

2.5. Antimicrobial studies

Antimicrobial activities of all complexes were determined based on a micro-well dilution assay [26] and described with some modifications as follows. Minimal inhibitory concentrations (MIC values) for each compound were determined against standard bacterial strains: *E. coli* (ATCC 25922), *B. subtilis* ATCC (21332) and one fungal strain: *C. albicans* (ATCC 60193) were obtained from İnönü University in Turkey. Bacterial and fungal microorganisms were sub-cultured in Luria-Bertani (LB) Broth (Sigma–Aldrich Chemie GmbH Taufkirchen, Germany). 1.6 mg of each compound was weighted and dissolved in (DMSO). Then, all of the dilutions were performed using distilled water. The initial concentrations of the tested compounds without adding bacterial and fungal cultures were 400, 200, 100, 75, 50 and 25 μg/mL. After adding bacterial and fungal cultures, the final concentrations of the tested compounds were 200, 100, 50, 37.5, 25 and 12.5 μg/mL. Cefotaxime was used as an antibacterial and antifungal standard drug, whose minimum inhibitory concentration (MIC) values are given in Table 3. The inoculated bacteria and yeast cultures were incubated at 37 °C until reaching 0.5 McFarland standard turbidity. After the incubation, 100 μl of the liquid cultures was added into each well of sterile 96-well plates containing different concentrations of 100 μl tested compounds. After 24 h incubation time, MIC values for the compounds were determined as in Table 3. The lowest concentration of the compounds that prevented from visible growth via measuring the absorbance at 625 nm was considered to be the minimal inhibitory concentration (MIC) value.

2.6. DNA interaction studies

2.6.1. Agarose gel electrophoresis method

The DNA interaction activities of the complexes were studied by agarose gel electrophoresis method using pBR322 plasmid DNA. The complexes were dissolved in DMSO. Then, the test samples were prepared in different final concentrations as 25, 50, 100 and 200 μg/ml by adding pBR322 plasmid DNA. After adding 4 μl of pBR322 (0.05 μg/ml) into each tube containing 4 μl of cisplatin as four controls and the test samples in different concentrations, we incubated them for 24 h at 37 °C. After incubation, the plasmid DNA sample was mixed with bromophenol blue dye (2 μl), loaded into the electrophoresis chamber wells along with the control DNA (0.05 μg/ml pBR322) and electrophoresed at 60 V for 40 min using 1% agarose gel. After running the gel, it was removed and stained with ethidium bromide solution and the image was taken in Syngene G:BOX gel documentation system.

The DNA interaction ability of the complexes was investigated using pBR322 DNA. It is well established that when circular plasmid DNA was subjected to gel electrophoresis, relatively fast migration was observed for the intact supercoiled form (I). If binding of DNA to the complex occurs, the supercoiled form (I) will move slowly compared to pBR322 without the complex.

2.6.2. UV–vis absorption studies and competitive displacement assay

Interaction mode of the complexes with *ct*DNA was explored using UV–vis absorption spectroscopy and ethidium bromide (EB) competitive displacement assay. All the absorption and fluorescence measurements were performed by using FS5 spectrofluoremeter. Absorption spectra of the studied systems were recorded between 350 and 600 nm. The measurements were carried on the fixed ethidium bromide and DNA concentrations. Various amount of Ru and Pd complexes were added onto the EB-*ct*DNA complex. All experiments were performed at room temperature.

In the competitive displacement assay, EB-*ct*DNA complex was formed by mixing the 1.97 μg/mL EB and 19.8 μg/mL *ct*DNA and the concentrations were fixed all along the experiments. Obtained EB-*ct*DNA complex was titrated by adding various amounts of Ru and Pd complexes on it. Fluorescence emission spectra were recorded between 500 and 800 nm upon excitation of the system at 526 nm.

3. Results and discussion

3.1. Synthesis and spectral characterization

Pd(II)–NHC complexes (**1a-d**) were synthesized by the reaction of corresponding imidazolium and benzimidazolium chlorides and $PdCl_2$. The carbene precursors were available from our previous study [21]. The reaction was carried out in pyridine at 80 °C for 3 h and K_2CO_3 was used as an external base. The crude products were re-crystallized from dichloromethane (DCM)/*n*-hexane and moderate yields were observed between 36 and 55%. Synthesis and structures of Pd(II)–NHC complexes are outlined in Scheme 1. The complexes were fully characterized by ^{1}H NMR, ^{13}C NMR, IR spectroscopic techniques and elemental analyses. Additionally, all spectral assignments were made with the help of COSY, HSQC and HMBC spectra of **1a** (See SI for spectra). In the ^{1}H NMR spectra of **1a-d**, the disappearance of downfield signals which had been observed in the range of 9.82–10.93 ppm [21] clearly indicates the deprotonation of carbene carbons. The signals of methylene hydrogens between two nitrogen atoms were observed as singlets in the range of 7.38–7.83 ppm. In the ^{13}C NMR spectra of **1a-d**, the resonances of carbene carbons were observed at 151.7 and 151.3 ppm for imidazole-based **1a,b** and at 164.8 and 166.1 ppm for benzimidazole-based **1c,d**, respectively and these signals are in agreement with the literature [17,27].

Ru(II)–NHC complexes (**3a-d**) were synthesized by the carbene transfer route. The used silver-NHCs (**2a-d**) were ready from our previous study [15]. Ru(II)–NHCs were synthesized in dry DCM and rigorous inert conditions in contrast to Pd(II)–NHCs. The target complexes were obtained in moderate yields between 39 and 57% by the reaction of corresponding silver(I)–NHCs and ruthenium *p*-cymene dimer in DCM at 40 °C for 24 h. Synthesis and structures of

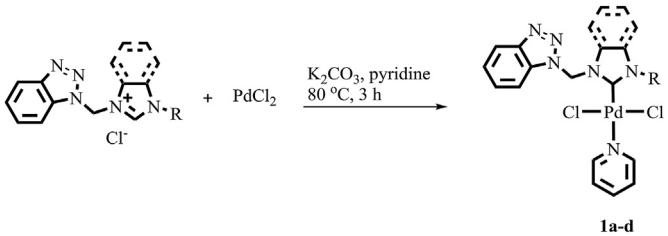

Scheme 1. Synthesis and structures of Pd(II)–NHCs, **1a-d**. **a**, imidazole, R = →CH_3; **b**, imidazole, R = $-CH_2CH_2CH_2CH_3$; **c**, benzimidazole, R = $-CH_2CH_2CH_2CH_3$; **d**, benzimidazole, R = $-CH_2C_6H_5$.

Ru(II)–NHCs are given in Scheme 2. The structures of complexes were established by ^{1}H NMR, ^{13}C NMR and IR spectroscopic techniques and elemental analyses. Spectral assignments were achieved with the help of COSY and HSQC spectra of **3b** (See SI for spectra). In the ^{1}H NMR spectra of **3a-d**, additional signals belong to *p*-cymene ring were observed as expected. Methylene hydrogens between two nitrogen atoms were observed as doublets in the range of 7.79–8.07 and 6.17–6.46 ppm with geminal coupling constants that 14.1 Hz for **3a** and 14.6, 14.6, and 14.5 Hz for **3b-d**, respectively. In the ^{13}C NMR spectra of **3a-d**, resonances of carbene carbons were observed at 173.3 ppm for imidazole-based **3a**, and 188.3, 189.8, and 189.9 ppm for benzimidazole-based **3b-d**, respectively.

The other observed signals of Pd(II)- and Ru(II)–NHCs in the ^{1}H and ^{13}C NMR spectra are in good agreement with expected integral values and coupling patterns. In addition, the results of elemental analysis are in accordance with the proposed structures. Suitable crystals for X-ray analysis were obtained by the slow diffusion of *n*-hexane into the concentrated DCM solution for **1c**.

3.2. Description of the crystal structure of 1c

An ORTEP-3 view of **1c** is shown in Fig. 1, and selected geometrical parameters obtained from X-ray analysis are listed in Table 1.

Analysis of the X-ray crystallographic data revealed that the compound crystallized in triclinic system space group $P\bar{1}$ with two molecules in the unit cell. The structure of **1c** consists of a square planar molecule with a palladium centre surrounded by a pyridine ring, two chloro ligands in the *trans* configuration, and NHC ligand. The Cl1–Pd1–Cl2 [179.52(3)°] and N6–Pd1–C14 [176.50(10)°] bond angles showed that there was slight distortion in the square planar coordination of metal centre. The Pd–$C_{carbene}$ and Pd–Cl bond lengths are quite similar to that shown by other palladium-related species [28]. The Pd–N_{py} bond length is longer than those shown for complexes with non-NHC ligands, representing the high *trans* influence of NHCs [29].

In the NHC ligand, the N=C imine bond lengths are shorter than the amine N–C bond lengths as expected, and the N–C–N bond angles are in good agreement with the typical angles of 104–107° known for NHCs [30]. In the benzotriazole rings, the bond lengths and angles agree well with standard values except for N–N bonds. The variation of N–N bonds is attributed to the tautomerism of the benzotriazole ring [31].

3.3. Cytotoxicity studies

The cytotoxic properties of all complexes were evaluated against human colorectal (Caco-2) and breast (MCF-7) cancer cell lines and non-cancer mouse fibroblast (L-929) cell lines. Cisplatin was used

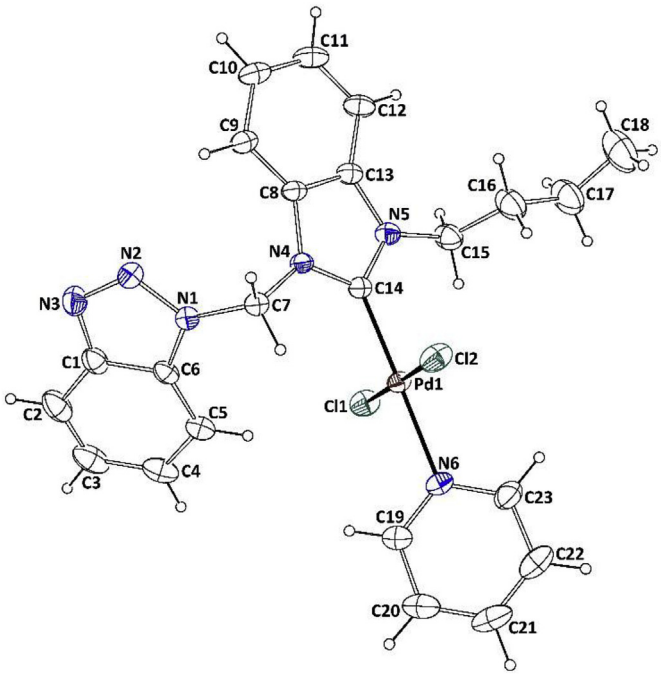

Fig. 1. The molecular structure of **1c** with thermal ellipsoids at 20% probability. H atoms are shown as small spheres of arbitrary radii and only the major part of the disordered fragment is shown.

Table 1
Selected geometric parameters for **1c**.

Bond lengths (Å)			
Pd1–C14	1.955(2)	N4–C7	1.450(3)
Pd1–N6	2.085(2)	N4–C14	1.355(3)
Pd1–Cl1	2.2931(8)	N5–C14	1.344(3)
Pd1–Cl2	2.3055(8)	N4–C8	1.397(3)
N1–N2	1.358(3)	N5–C13	1.396(3)
N3–N2	1.298(4)	N6–C19	1.308(4)
N1–C6	1.364(3)	N6–C23	1.326(4)
N3–C1	1.378(5)	N5–C15	1.457(4)
N1–C7	1.440(3)		
Bond angles (°)			
C14–Pd1–N6	176.50(10)	N4–C14–N5	106.9(2)
Cl1–Pd1–Cl2	179.52(3)	N2–N1–C7	119.7(2)
C14–Pd1–Cl1	91.15(7)	N3–N2–N1	108.5(2)
C14–Pd1–Cl2	88.41(7)	C19–N6–Pd1	120.4(2)
N6–Pd1–Cl1	91.79(7)	N5–C14–Pd1	126.91(19)
N6–Pd1–Cl2	88.64(7)	N4–C14–Pd1	125.94(17)
N1–C7–N4	113.3(2)	C14–N5–C15	125.5(2)

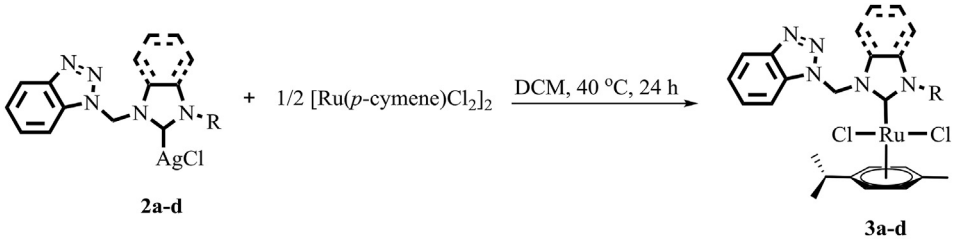

Scheme 2. Synthesis and structures of Ru(II)–NHCs, **3a-d**. **a**, imidazole, R = →$CH_2CH_2CH_2CH_3$; **b**, benzimidazole, R = –$CH_2CH_2CH_2CH_3$; **c**, benzimidazole, R = –$CH_2C_6H_5$; **d**, benzimidazole, R = –$CH_2C_6H_5$-3,4,5-$(OCH_3)_3$.

as the standard for comparison. IC_{50} values of all complexes and cisplatin after 24 h of incubation time are listed in Table 2. Morphological changes of cells after 24 h of treatment of complex solutions were monitored by inverted microscope (Fig. S16-S18).

When the results were evaluated, it was observed that Ru(II)–NHCs are more cytotoxic against Caco-2 and MCF-7 cancer cell lines than Pd(II)–NHCs. Among all the complexes, only benzyl-substituted benzimidazole-based Ru–NHCs, **3c** and **3d** performed comparable cytotoxicity with cisplatin against Caco-2 cell lines. These complexes did not show cytotoxicity against non-cancer L-929 cell lines. In our previous study, we had reported that **2c**, the corresponding silver-NHC of **3c** was a promising candidate for the treatment of human colorectal and breast cancers. **2c** had performed much more cytotoxicity against Caco-2 and MCF-7 cell lines than cisplatin, however, cytotoxicity of **2c** was stronger than cisplatin against non-cancer L-929 [15]. When the cytotoxic properties of ruthenium-NHC complexes compared with literature, we must note that more active complexes were reported previously by other groups. For example, Tacke and co-workers reported the synthesis and anticancer properties of highly lipophilic ruthenium-NHCs and three of those complexes performed stronger cytotoxic properties against MCF-7 cell lines than cisplatin [32].

In the cancer treatment, platinum complexes are the most used metal-based anticancer agents. However, they have some limitations such as toxicity and resistance for application [2]. In addition to the activities of drugs, their selectivity is also highly important for the prevention of side effects in the treatment. Therefore, alternative metallopharmaceuticals are being investigated for platinum complexes, and the ruthenium complexes are one of these candidates. Moreover, it is also an important advantage that ruthenium-NHCs were reported as less toxic than the corresponding gold-NHCs [19]. If we evaluate the findings of this study based on above information, we think that the selectivity of **3c** and **3d** against human colorectal cancer cells is an advantage compared with cisplatin and corresponding silver-NHCs.

3.4. Antimicrobial studies

Antimicrobial activities of all complexes were tested against *E. coli*, (Gram-negative), *B. subtilis* (Gram-positive), and *C. albicans* as fungi. The minimum inhibitory concentration (MIC) values of all complexes at 24 h were listed in Table 3. Cefotaxime was used standard for comparison. As seen from Table 3, all complexes inhibited the growth of bacterial and fungi strains with 100 or 200 μg/mL MIC values. The obtained results are comparable with their carbene precursors and Cefotaxime but corresponding silver-NHCs had performed much better activity than **1a-d** and **3a-d** [15]. As we previously mentioned, palladium and ruthenium complexes are not strong antimicrobial agents in literature and these results are not surprising. The non-promising results led us to concentrate more on the anticancer effects of complexes [15].

Table 2
IC_{50} values (μM) of complexes at 24 h.

Compound	Caco-2	MCF-7	L-929
1a	376 ± 52	530 ± 2	N.D.
1b	N.D.	210 ± 41	231 ± 1
1c	219 ± 27	192 ± 8	N.D.
1d	162 ± 5	410 ± 5	221 ± 15
3a	201 ± 11	407 ± 66	51 ± 1
3b	158 ± 11	256 ± 39	75 ± 1
3c	100 ± 7	137 ± 2	N.D.
3d	90 ± 1	270 ± 12	N.D.
Cisplatin	76 ± 6	81 ± 1	46 ± 7

N.D.: Not Determined.

Table 3
MIC values (μg/mL) of complexes at 24 h.

Compound	*Escherichia coli* (Gram-negative)	*Bacillus subtilis* (Gram-positive)	*Candida albicans* (Fungi)
1a	100	200	200
1b	100	200	200
1c	200	200	200
1d	200	200	200
3a	100	200	200
3b	200	200	200
3c	200	100	200
3d	100	200	200
Cefotaxime	250	250	250

3.5. DNA interaction studies

DNA interaction studies were carried out by using two different model system. Firstly, agarose gel electrophoresis was performed to investigate the ability of synthesized palladium and ruthenium NHC complexes to interact with the supercoiled (SC) pBR322 plasmid DNA. The influence of the complex on the structure of DNA can be evaluated by their DNA-interaction ability. The mobility behaviours of the pure plasmid DNA, the plasmid DNA with cisplatin as controls and the plasmid DNA treated with the complexes in increasing amounts as 50 and 100 μg/ml final concentrations of the sample with pBR322 plasmid DNA (0.025 μg/μl final concentration in the solution) are shown in Fig. 2 and Fig. 3.

The concentration-dependent retardation in the supercoiled plasmid DNA mobility is observed due to the binding of ruthenium complexes in different concentrations from Fig. 3. With increasing concentrations of ruthenium NHC complexes especially for 3c and 3d, supercoiled forms (I) of the plasmid move slowly compared to the pure pBR322 plasmid DNA (lanes 1 and 2). On the other hand, palladium NHC complexes, unlike ruthenium NHC complexes, have no binding ability to the plasmid DNA. From Fig. 2 with increasing concentrations of palladium complexes except 1d complex, which has an oxidation also known as negative effect over plasmid DNA, supercoiled forms (I) of the plasmid are on the same level as pure pBR322 plasmid DNA bands (lanes 1 and 2). Moreover, cisplatin controls for palladium and ruthenium complexes (lanes 3 and 4) have also effects on both supercoiled form (I) and nicked circular form (II) compared to the pure pBR322 plasmid (lanes 1 and 2 both for Figs. 2 and 3). Ruthenium complexes have been known for the generation of reactive oxygen species (ROS). As it can be realized from Fig. 3, band intensities of the only plasmid pBR322 (lanes 1 and 2) are slightly brighter than the ruthenium complexes, which indicates ROS generation by these complexes [33].

Secondly, UV–vis absorption studies were performed to remarkable information about the interaction mode of the small molecules with double-stranded DNA. EB is a well-known intercalative DNA binding probe [34]. Addition of *ct*DNA on EB solution resulted in hypochromism and slight red shift at absorption maxima of the EB, which is the characteristic behaviour of the intercalative binding. Effect of the various amounts of the Ru complexes (3c and 3d) on the EB-*ct*DNA system were investigated and the decrease in absorption values was observed (Fig. 4b and d.). This behaviour can be considered as intercalative binding continues after displacement of the EB with Ru complexes. Addition of various amount of the Pd complex on the EB-*ct*DNA system resulted in hyperchromocity and the disappearing of the characteristic shape of the absorption band (Fig. S19).

To further examination of the binding mode of ruthenium and palladium complexes with *ct*DNA, a series of competitive displacement assays were carried out with EB. The weak fluorescence intensity of the EB increases upon intercalation between base

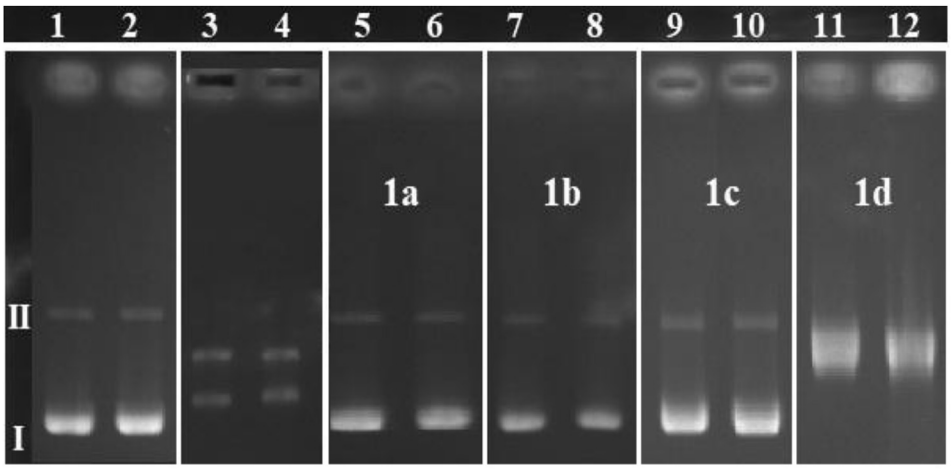

Fig. 2. The above agarose gel electrophoresis showing changes in electrophoretic mobility of the super helicoidal form (I) and the open circular form (II) of only plasmid pBR322 (0.025 μg/μl) (lanes 1 and 2) and plasmid pBR322 (0.025 μg/μl final concentration in the solution) (lanes 3–12) after incubation (24 h at 37 °C) with 50 and 100 μg/ml cisplatin controls (lanes 3 and 4), 50 and 100 μg/ml final concentrations of **1a-d** palladium NHC complexes (lanes 5–12), respectively.

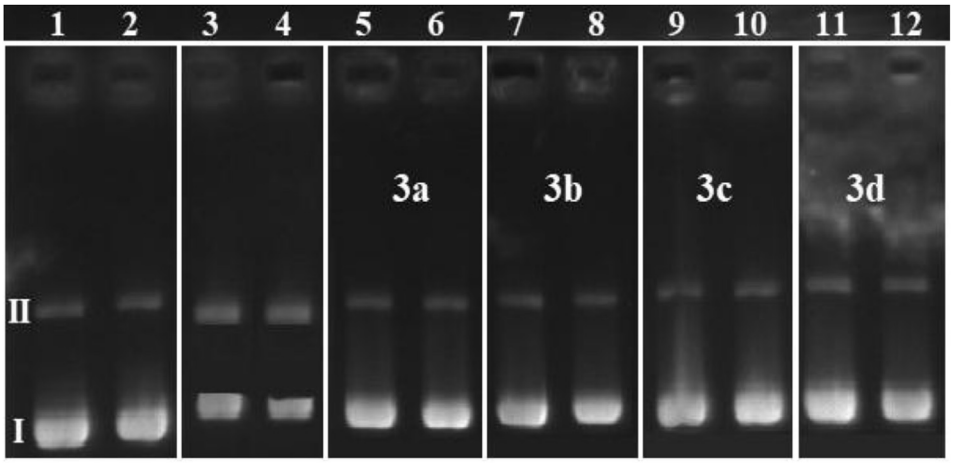

Fig. 3. The above agarose gel electrophoresis showing changes in electrophoretic mobility of the super helicoidal form (I) and the open circular form (II) of only plasmid pBR322 (0.025 μg/μl) (lanes 1 and 2) and plasmid pBR322 (0.025 μg/μl final concentration in the solution) (lanes 3–12) after incubation (24 h at 37 °C) with 50 and 100 μg/ml cisplatin controls (lanes 3 and 4), 50 and 100 μg/ml final concentrations of 3a-d ruthenium NHC complexes (lanes 5–12), respectively.

pairs of *ct*DNA. However, the enhanced fluorescence can be quenched evidently when there is a second molecule that can replace DNA-bound EB [35]. Effects of the ruthenium complexes (3c and 3d) on the fluorescence emission of the EB-*ct*DNA system are shown in Fig. 4a and c. The fluorescence titration results were analysed by using Stern-Volmer equation (1) and the K_{SV} values of EB-ctDNA in the presence of the ruthenium complexes were calculated the slope of the graphs [36];

$$F_0/F = 1 + K_{sy}[Q]$$

F_0 and F represent the steady-state fluorescence intensities of EB-*ct*DNA in the absence and presence of the ruthenium complexes, respectively. [Q] refers to the concentration of complexes as a quencher. K_{sv} indicates the Stern–Volmer quenching constant.

Ruthenium complex additions resulted in the decrease of the fluorescence intensity gradually. These results suggested that the ruthenium complexes could interact with DNA via a similar intercalative mode and was able to replace EB being sandwiched between adjacent base pairs of the *ct*DNA duplex. Addition of the palladium complex didn't cause any significant change in the fluorescence emission of the EB-*ct*DNA system (Fig. S19). It can be considered that there is not binding in an intercalative manner. The results are consistent with the UV–vis absorption studies.

4. Conclusion

In conclusion, we reported the synthesis, characterization and biological investigation of palladium(II) and ruthenium(II) complexes with benzotriazole functionalized NHC ligands. Antimicrobial studies showed that the complexes are not promising antimicrobial agents. DNA interaction studies revealed that these complexes have weaker DNA binding ability compared to cisplatin. On the other hand, two ruthenium(II)–NHC complexes, **3c** and **3d** performed comparable cytotoxicity against Caco-2 cancer cell lines with cisplatin. At the same time, these complexes were found out as non-cytotoxic against non-cancer L-929 cells. Even if there are no high cytotoxic properties of the complexes reported here, functionalization of Ru–NHCs may contribute to selectivity against different cell lines.

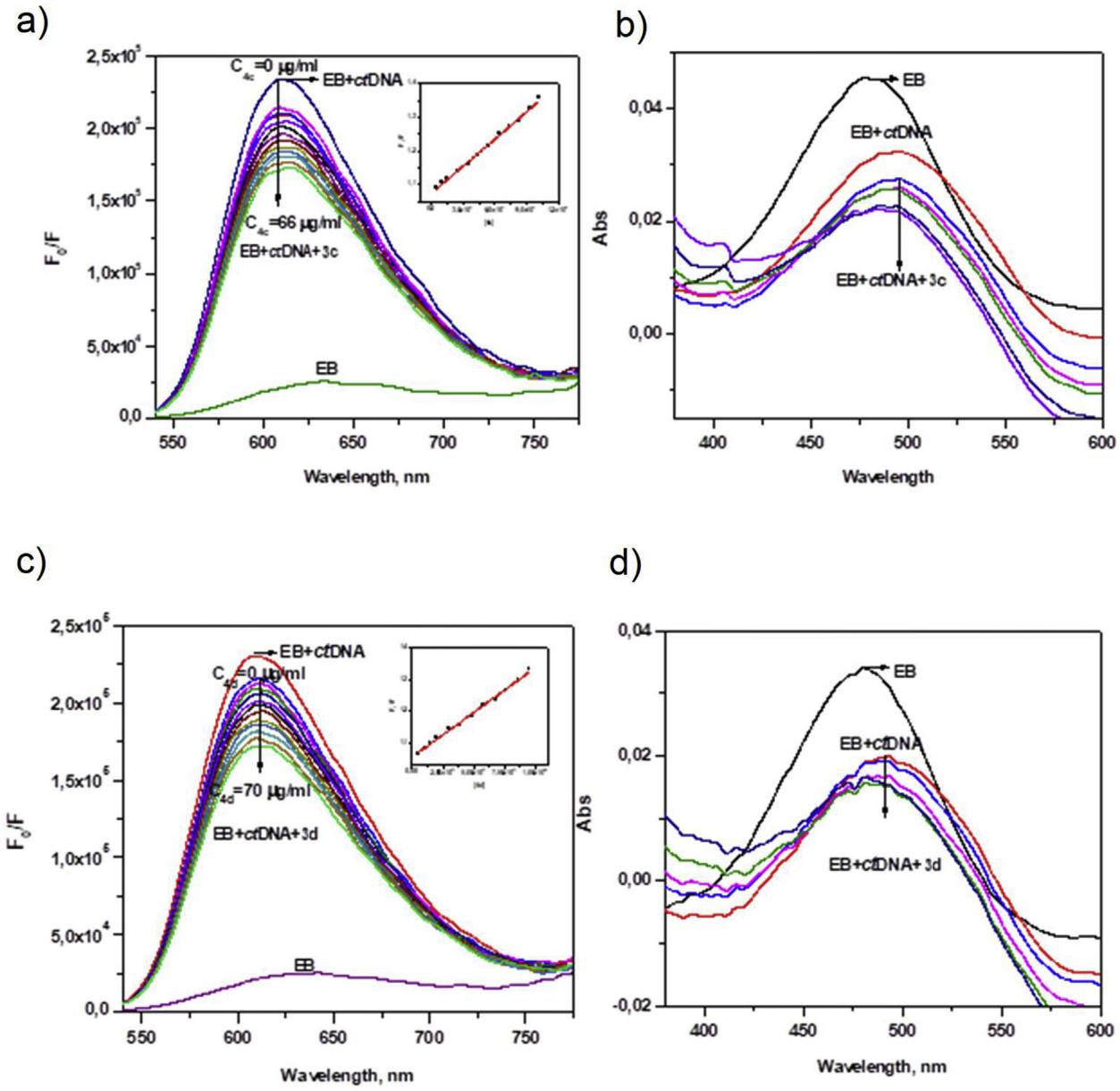

Fig. 4. Effect of the ruthenium complexes **3c** and **3d** on the **(a;c)** fluorescence emission and **(b;d)** absorption of the EB-*ct*DNA complex.

Acknowledgments

The authors report no conflicts of interest. The authors alone are responsible for the content and writing of the paper.

Appendix A. Supplementary data

Supplementary data to this article can be found online at https://doi.org/10.1016/j.jorganchem.2019.02.013.

References

[1] B. Rosenberg, L. Vancamp, J.E. Trosko, V.H. Mansour, Platinum compounds: a new class of potent antitumour agents, Nature 222 (1969) 385–386.
[2] S. Medici, M. Peana, V.M. Nurchi, J.I. Lachowicz, G. Crisponi, M.A. Zoroddu, Noble metals in medicine: latest advances, Coord. Chem. Rev. 284 (2015) 329–350.
[3] A.L. Noffke, A. Habtemariam, A.M. Pizarro, P.J. Sadler, Designing organometallic compounds for catalysis and therapy, Chem. Commun. 48 (2012) 5219–5246.
[4] W. Liu, R. Gust, Update on metal N-heterocyclic carbene complexes as potential anti-tumor metallodrugs, Coord. Chem. Rev. 329 (2016) 191–213.
[5] H.W. Wanzlick, H.J. Schönherr, Direct synthesis of a mercury salt-carbene complex, Angew. Chem. Int. Ed. 7 (1968) 141–142.
[6] K. Öfele, , 1,3-Dimethyl-4-imidazolinyliden-(2-)pentacarbonylchrom, J. Organomet. Chem. 12 (1968) 42–43.
[7] A.J. Arduengo, R.L. Harlow, M. Kline, A stable crystalline carbene, J. Am. Chem. Soc. 113 (1991) 361–363.
[8] W.A. Herrmann, N-Heterocyclic carbenes: a new concept in organometallic catalysis, Angew. Chem. Int. Ed. 41 (2002) 1290–1309.
[9] B. Çetinkaya, E. Çetinkaya, H. Küçükbay, R. Durmaz, Antimicrobial activity of carbene complexes of rhodium(I) and ruthenium(II), Arzneim.-Forsch./Drug Res. 46 (1996) 821–823.
[10] A. Melaiye, R.S. Simons, A. Milsted, F. Pingitore, C. Westemiotis, C.A. Tessier, W.J. Youngs, Formation of water-soluble Pincer silver(I)-carbene complexes: a novel antimicrobial agent, J. Med. Chem. 47 (2004) 973–977.
[11] P.J. Barnard, M.V. Baker, S.J. Berners-Price, D.A. Day, Mitochondrial permeability transition induced by dinuclear gold(I)-carbene complexes: potential new antimitochondrial antitumour agents, J. Inorg. Biochem. 98 (2004) 1642–1647.
[12] (a) M.E. Garner, W. Niu, X. Chen, I. Chiviriga, K.A. Abboud, W. Tan, A.S. Veige, N-Heterocyclic carbene gold(I) and silver(I) complexes bearing functional

groups for bio-conjugation, Dalton Trans. 44 (2015) 1914–1923;
(b) C.V. Maftei, E. Fodor, P.G. Jones, M. Freytag, M.H. Franz, G. Kelter, H.H. Fiebig, M. Tamm, I. Neda, N-Heterocyclic carbenes (NHC) with 1,2,4-oxadiazole-substituents related to natural products: synthesis, structure and potential antitumor activity of some corresponding gold(I) and silver(I) complexes, Eur. J. Med. Chem. 101 (2015) 431–441;
(c) M.O. Karataş, B. Olgundeniz, S. Günal, İ. Özdemir, B. Alıcı, E. Çetinkaya, Synthesis, characterization and antimicrobial activities of novel silver(I) complexes with coumarin substituted N-heterocyclic carbene ligands, Bioorg. Med. Chem. 24 (2016) 643–650.

[13] I. Briguglio, S. Piras, P. Corona, E. Gavini, M. Nieddu, G. Boatto, A. Carta, Benzotriazole: an overview on its versatile biological behaviour, Eur. J. Med. Chem. 97 (2015) 612–648.

[14] (a) Z. He, S.F. Zhang, J.R. Xue, Y. Liang, X. Zhang, L.H. Jing, D.B. Qin, Verstile silver(I) and nickel(II) NHC complexes bearing benzotriazole-function: synthesis, fluorescence and catalytic properties, J. Organomet. Chem. 808 (2016) 12–22;
(b) M. Monticelli, S. Bellemin-Laponnaz, C. Tubaro, M. Rancan, Synthesis, structure and antitumoural activity of triazole functionalized NHC-metal complexes, Eur. J. Inorg. Chem. 2017 (2017) 2488–2495.

[15] G. Onar, M.O. Karataş, S. Balcıoğlu, T.T. Tok, C. Gürses, I. Kılıç-Cıkla, N. Özdemir, B. Ateş, B. Alıcı, Benzotriazole functionalized N-heterocyclic carbene-silver(I) complexes: synthesis, cytotoxicity, antimicrobial, DNA binding and molecular docking studies, Polyhedron 153 (2018) 31–40.

[16] L. Oehninger, M. Stefanopovlou, H. Alborzinia, J. Schur, S. Ludewig, K. Namikawa, A. Munoz-Castro, R.W. Köster, K. Baumann, S. Wolfl, W.S. Sheldrick, I. Ott, Evaluation of arene ruthenium(II) N-heterocyclic carbene complexes as organometallics interacting with thiol and selenol containing biomolecules, Dalton Trans. 42 (2013) 1657–1666.

[17] S. Ray, R. Mohan, J.K. Singh, M.K. Samantaray, M.M. Shaikh, D. Panda, P. Ghosh, Anticancer and antimicrobial metallopharmaceutical agents based on palladium, gold, and silver N-heterocyclic carbene complexes, J. Am. Chem. Soc. 129 (2007) 15042–15053.

[18] A. Bergamo, G. Sava, Ruthenium anticancer compounds: myths and realities of the emerging metal-based drugs, Dalton Trans. 40 (2011) 7817–7823.

[19] O. Çiftçi, İ. Özdemir, O. Çakır, S. Demir, The determination of oxidative damage in heart tissue of rats caused by ruthenium(II) and gold(I) N-heterocyclic carbene complexes, Toxicol. Ind. Health 27 (2011) 735–741.

[20] M.L. Teyssot, A.S. Jarrousse, M. Manin, A. Chevry, S. Roche, F. Norre, C. Beaudoin, L. Morel, D. Boyer, R. Mahiou, A. Gautier, Metal-NHC complexes: a survey of anti-cancer properties, Dalton Trans. 2009 (2009) 6894–6902.

[21] M.O. Karataş, H. Uslu, B. Alıcı, B. Gökçe, N. Gençer, O. Arslan, N.B. Arslan, N. Özdemir, Functionalized imidazolium and benzimidazolium salts as paraoxonase I inhibitors: synthesis, characterization and molecular docking studies, Bioorg. Med. Chem. 24 (2016) 1392–1401.

[22] Stoe & Cie, X-AREA Version 1.18 and X-RED32 Version 1.04, Stoe & Cie, Darmstadt, Germany, 2002.

[23] G.M. Sheldrick, SHELXT- Integrated space-group and crystal-structure determination, Acta Crystallogr. A 71 (2015) 3–8.

[24] G.M. Sheldrick, Crystal structure refinement with SHELXL, Acta Crystallogr. C 71 (2015) 3–8.

[25] L.J. Farrugia, WinGX and ORTEP for windows: an update, J. Appl. Crystallogr. 45 (2012) 849–854.

[26] J.R. Zgoda, J.R. Porter, A convenient microdilution method for screening natural products against bacteria and fungi, Pharm. Biol. 39 (2001) 221–225.

[27] N. Kaloglu, M. Kaloglu, M.N. Tahir, C. Arıcı, C. Bruneau, H. Doucet, P.H. Dixneuf, B. Çetinkaya, İ. Özdemir, Synthesis of N-heterocyclic carbene-palladium-PEPPSI complexes and their catalytic activity in the direct C-H bond activation, J. Organomet. Chem. 867 (2018) 404–412.

[28] (a) X.X. He, Y. Li, B.B. Ma, Z. Ke, F.S. Liu, Sterically encumbered tetrarylimidazolium carbene Pd-PEPPSI complexes: highly efficient direct arylation of imidazole with aryl bromides under aerobic conditions, Organometallics 35 (2016) 2655–2663;
(b) C.H. Ke, B.C. Kuo, D. Nandi, H.M. Lee, Monodentate palladium complexes bearing abnormal and normal carbene ligands with a formally identical steric environment, Organometallics 32 (2013) 4775–4784;
(c) A. Zanardi, J.A. Mata, E. Peris, Domino approach to benzofurans by the sequential Sonogashira/Hydroalkoxylation couplings catalysed by new N-heterocyclic-carbene-palladium complexes, Organometallics 28 (2009) 4335–4339.

[29] (a) Z.D. Bugarcic, B. Petrovic, E. Zangrando, Kinetics and mechanism of the complex formation of $[Pd(NNN)Cl]^{+}$ with pyridines in methanol: synthesis and crystal structure of $[Pd(terpy)(py)](ClO_4)_2$, Inorg. Chim. Acta 357 (2004) 2650–2656;
(b) D. Jaganyi, F. Tiba, O.Q. Munro, B. Petrovic, Z.D. Bugarcic, Kinetic and mechanistic study on the reactions of $[Pt(bpma)(H_2O)]^{2+}$ and $[Pd(bpma)(H^2O]^{2+}$ with some nucleophiles. Crystal structure of $[Pd(bpma)(py)](ClO_4)_2$, Dalton Trans. 24 (2006) 2943–2949.

[30] Y. Li, X. Chen, Y. Song, L. Fang, G. Zou, Well-defined N-heterocyclic carbene silver halides of 1-cyclohexyl-3-arylmethylimidazolylidenes: synthesis, structure and catalysis in A^3-reaction of aldehydes, amines and alkynes, Dalton Trans. 40 (2011) 2046–2052.

[31] V.N. Mikhaylov, V.N. Sorokoumov, K.A. Korvinson, A.S. Novikov, I.A. Balova, Synthesis and simple immobilization of palladium(II) acyclic diaminocarbene complexes on polystyrene support as efficient catalysts for Sonogashira and Suzuki-Miyaura couplings, Organometallics 35 (2016) 1684–1697.

[32] F. Hackenberg, H. Müller-Bunz, R. Smith, W. Streciwilk, X. Zhu, M. Tacke, Novel ruthenium(II) and gold(I) NHC complexes: synthesis, characterization, and evaluation of their anticancer properties, Organometallics 32 (2013) 5551–5560.

[33] F.D. Abreu, T.F. Paulo, M.H. Gehlen, R.A. Ando, L.G.F. Lopes, A.C.S. Gondim, M.A. Vasconcelos, E.H. Teixeria, E.H.S. Sousa, I.M.M. Carvalho, Aryl-substituted ruthenium(II) complexes: a strategy for enhanced photocleavage and efficient DNA binding, Inorg. Chem. 56 (2017) 9084–9096.

[34] H.G. Li, Z.Y. Yang, B.D. Wang, J.C. Wu, Synthesis, crystal structure, antioxidation and DNA-binding properties of the Ln complexes with 1-phenyl-3-methyl-hydroxypyrazole-4-carbaldhyde-(benzoyl)hydrazine, J. Organomet. Chem. 695 (2010) 415–422.

[35] I. Ahmad, A. Ahmad, M. Ahmad, Binding properties of pendimethalin herbicide to DNA: multispectroscopic and molecular docking approaches, Phys. Chem. 18 (2016) 6476–6485.

[36] J.R. Lakowicz, Principles of Fluorescence Spectroscopy, third ed., Springer, New York, 2006.